applied sciences

MDPI

Article

Design and Realization of an Ultra-Wideband, Pattern-Stable Antenna for Ground Sensing Applications with UAVs

Daniele Pinchera [1,2], Fulvio Schettino [1,2], Mario Lucido [1,3,*], Gaetano Chirico [1,2] and Marco Donald Migliore [1,2]

[1] DIEI, University of Cassino and Southern Lazio, Via G. Di Biasio 43, 03043 Cassino, Italy; pinchera@unicas.it (D.P.); schettino@unicas.it (F.S.); gaetano.chirico@unicas.it (G.C.); mdmiglio@unicas.it (M.D.M.)
[2] European University of Technology EUt+, European Union, B-1049 Brussels, Belgium
[3] EUt+ Institute of Nanomaterials and Nanotechnologies—EUTINN, European University of Technology, European Union, B-1049 Brussels, Belgium
* Correspondence: lucido@unicas.it

Abstract

The present work addresses the critical challenge of designing a lightweight antenna suitable for remote sensing applications specifically aimed at the identification of buried objects from Unmanned Aerial Vehicles (UAVs). The stability of the phase center and the radiation pattern are critical factors for enabling synthetic aperture radar (SAR) processing on moving platforms. The presented antenna structure is characterized by a simple, lightweight geometry, and allows for achieving a fractional bandwidth of nearly 100% with an excellent stability of the radiation pattern, that exhibits minimal variation within the operating band of the antenna. Specifically, the gain is in the range 4.4–6.3 dBi and the group delay spread is about 200 ps in the frequency range 1–2 GHz. We illustrate numerical simulations and measurements of an antenna prototype that validate the proposed approach, demonstrating the suitability of the design for the intended operational scenario.

Keywords: unmanned aerial vehicle (UAV); ground penetrating radar (GPR); ultra-wideband (UWB) antenna; buried object detection; remote sensing; lightweight antenna; pattern stability

1. Introduction

The detection and localization of buried objects remain a critical challenge across various fields, including humanitarian demining, archaeological prospecting, and civil engineering. Humanitarian demining operations urgently require low-cost, easy-to-use, and efficient technologies to improve the mapping of hazardous areas while ensuring operator safety. Within this framework, Ground Penetrating Radar (GPR) has emerged as a key sensing technology for detecting, imaging, and identifying subsurface buried structures [1].

GPR systems operate by detecting dielectric discontinuities in the propagation medium, sensing backscattered electromagnetic waves generated by electrical inhomogeneities—such as metal triggers, explosives, or the mine casing itself—against the surrounding soil [2]. The efficacy of this method relies heavily on the contrast between the target and the background medium, as well as the ability of the radar system to resolve small features at depth. Despite its potential, the practical deployment of GPR faces significant challenges, primarily related to false alarm rates and operational trade-offs. Handheld dual-sensor systems (e.g., HSTAMIDS and MINEHOUND), which combine GPR with

Academic Editor: Atsushi Mase

Received: 24 December 2025
Revised: 14 January 2026
Accepted: 20 January 2026
Published: 23 January 2026

metal detectors (MD) to mitigate the limitations of individual sensors, have shown improved performance in conflict zones. However, these solutions rely on manual scanning, exposing deminers to high risks and failing to exploit the full 3D imaging capabilities of radar. Conversely, vehicle-based array systems offer higher speeds (up to 10 km/h) but often lack high-resolution 3D imaging, leading to persistent false alarms. Previous attempts at airborne GPR, such as the Mineseeker airship project, maximized safety and coverage speed but struggled to reliably detect individual antipersonnel mines due to altitude constraints.

Consequently, the integration of GPR systems with Unmanned Aerial Vehicles (UAVs) has emerged as a transformative solution [3]. However, this transition introduces severe constraints regarding payload weight and electromagnetic performance. Unlike ground vehicles, UAVs have limited battery life and lift capacity, meaning that every gram of payload must be justified by performance. A major technological bottleneck lies in the hardware architecture of current commercial GPRs. The vast majority employ fixed RF electronics based on impulse radar technology [4–6]. These systems typically suffer from poor adaptability to different target sizes and soil conditions, and their significant weight and bulk hinder integration into lightweight Unmanned Aerial Vehicles (UAVs).

In the recent literature, the trade-offs associated with air-launched GPR have been extensively explored. A primary challenge is the development of effective imaging algorithms that can handle the complex scattering environment from a moving platform. Garcia-Fernandez et al. [7] demonstrated the feasibility of using synthetic aperture radar (SAR) processing on UAVs to detect buried landmines. Their work highlighted that while SAR can significantly improve resolution, accurate motion compensation and clutter removal are essential to mitigate the strong reflections from the air–soil interface. Crucially, SAR algorithms assume a stable phase center of the antenna over the frequency bandwidth. If the radiation pattern or the phase center shifts significantly with frequency, the focused image becomes blurred, reducing the detection probability [8]. Therefore, the antenna design is not merely a component choice but a fundamental enabler of the advanced signal processing required for successful detection.

To enable these sophisticated processing techniques, the physical antenna design must ensure high signal fidelity while adhering to strict weight limits. It is worth underlining that there is a large literature on antennas for UAVs [9–11], but most of the investigation has been focused on communication antennas, and the requirements for this application are usually less stringent with respect to object detection or imaging.

In fact, the use of wideband and ultra-wideband (UWB) systems requires particular attention to the characteristics, bandwidth, and directional properties of the signals. A comprehensive analysis of this domain is discussed in [12], where the authors provide a survey of the current landscape of UWB radar applications, outlining the critical developments in radio chips, standards, and signal processing techniques necessary for future research. However, the practical implementation of these systems imposes strict requirements on signal integrity and spectral compliance; these topics are addressed in [13], where the authors investigate UWB signal transmission within the framework of European regulations, demonstrating how specific pulse shaping strategies are essential to minimize waveform distortion.

Moreover, previous studies have shown that a wide and frequency-stable pattern improves buried object detection and reduces artifacts in the imaging process, due to a reduced pulse distortion [14–16]. For this reason, a stable behavior of the pattern in the frequency domain is a very desirable feature of imaging and detection systems.

For instance, Burr et al. [16] addressed this hardware challenge by investigating lightweight broadband antennas, explicitly focusing on Log-Periodic Dipole Arrays (LPDA)

and Transversal Electromagnetic (TEM) horn antennas. By utilizing 3D-printing technology for the antenna structures, they successfully reduced the system weight without compromising the broad bandwidth required for high-resolution depth profiling. However, 3D printing often requires specialized conductive filaments or post-processing plating, which can complicate the manufacturing process. Simple planar structures offer an alternative, but often lack the necessary directionality to avoid interference from the drone's electronics.

Beyond the antenna element itself, the integration of the radar with the UAV platform presents unique system-level challenges, particularly regarding the interaction with the ground surface. Wu and Lambot [17] provide a comprehensive analysis of a drone-borne GPR system, emphasizing the importance of full-wave modeling in accurately retrieving soil properties, such as moisture content. Their research illustrates that understanding the antenna's behavior in the presence of the ground is crucial for distinguishing between soil clutter and actual buried targets. Furthermore, advanced detection capabilities are being explored through the use of array configurations and polarimetric diversity. Schartel et al. [18] expanded on the potential of UAV-based systems for landmine detection, investigating how specific antenna configurations can enhance target classification in varying soil conditions [19].

From this perspective, SDR architectures provide a flexible, cost-effective, and lightweight alternative to traditional fixed hardware, enabling the development of adaptable radar prototypes suitable for UAV integration [20,21]. This approach aims to provide a safe and efficient solution for landmine detection, a critical necessity in highly affected regions, where hazardous areas still pose a threat to the civilian and military population.

This paper builds upon these foundational works by proposing the design of a lightweight antenna to be used in a non-invasive radar system based on Software-Defined Radio (SDR) technology for UAVs. In particular, the design of the antenna has been focused on three key parameters: a lightweight design, a large operational bandwidth (characterized by a low reflection coefficient in the range of 1–2 GHz), and stable pattern behavior within the working range. These specifications are derived directly from the operational needs of airborne GPR: the weight limit ensures longer flight times, the bandwidth allows for sufficient range resolution, and the pattern stability supports SAR processing. Unlike complex Vivaldi arrays or heavy commercial shielded units [3], the proposed solution employs a hybrid approach combining printed technology with a simple metallic corner reflector, and would be particularly beneficial for a non-invasive radar system based on SDR.

This work is organized as follows: Section 2 discusses the design of the antenna and its numerical optimization. In Section 3, the construction of the antenna prototypes is described, and we show the results of the measurements of the built prototype. Conclusions follow.

2. Design and Numerical Optimization

In this section, we describe the design of the antennas aimed at verifying the specifications discussed in the introduction. In particular, in accordance with the findings of the bibliographic search, to better satisfy the requirements of lightweight and compactness, we focused our attention on printed antenna technology. Printed antennas, being built on thin dielectric substrates, can guarantee a very low weight, and are usually available in various shapes that allow their adoption in a wide range of applications [22]. This versatility makes them ideal candidates for UAV payloads, where aerodynamic profile and mass distribution are of paramount importance.

It is worth considering the case of monopole-like antennas [23,24], which use print technology and are able to provide ultra-large bandwidths. However, their radiation pattern is usually close to omnidirectional, and this feature does not suit the operation on

UAVs due to possible interferences. Omnidirectional radiation not only wastes energy by transmitting it away from the ground but also increases the likelihood of picking up noise from the UAV motors and control electronics.

Unfortunately, when the antenna is realized using a background plane (patch antennas), it is possible to realize a pattern in a specific direction (suitable for avoiding interference from UAVs and other installed equipment), but the achieved bandwidth is usually small. On the other hand, when not using a background plane, the bandwidth can be larger; however, we suffer from a substantial variation of the beam shape with frequency changes [25–28].

A possible solution to these limitations may be the use of a cavity-backed antenna, which could help improve the radiation properties of the antenna [15,29,30]. Some designs of cavity-backed antennas can achieve good performance without negatively influencing the achieved bandwidth. Unfortunately, the satisfaction of the requirements of a UAV antenna for ground detection is not feasible with the classical cylindrical or parallelepiped cavity; for this reason, we have introduced a novel design, based on the use of a corner reflector, in close connection with the printed antenna, that realizes a non-resonating triangular-shaped cavity.

The choice of a non-resonating structure is essential for GPR applications. High-Q cavities store energy and release it slowly, causing resonance artifacts in the time domain. In a radar system, this phenomenon manifests as "ringing", which effectively blinds the receiver for a duration proportional to the Q-factor of the antenna, making the detection of shallow objects nearly impossible. By employing a wide-angle corner reflector, the structure behaves more like a directional baffle than a resonant cavity, preserving the short pulse duration (in time domain) or the wideband phase linearity (in frequency domain) required for imaging.

From a mechanical point of view, the corner reflector ensures a reduced use of metal panels, which can be realized with smaller thicknesses thanks to the geometrical robustness of the triangular shape. Moreover, due to the absence of a resonance, it is possible to achieve extremely wide bandwidths.

2.1. Antenna Optimization

In Figure 1, we can see the result of an extensive numerical investigation, in which a large number of structures has been tested and optimized using the full-wave electromagnetic simulation software "CST Studio Suite" [31]. In particular, we use its time-domain solver, which discretizes the 3D model of the antenna into a structured hexahedral mesh (a grid of small cuboids), calculating the propagation of electromagnetic fields step-by-step through time. This solver is particularly well-suited for broadband structures, as it can obtain the frequency response over the entire band of interest with a single simulation run using a Gaussian pulse excitation. The size of the discretization mesh is chosen to ensure the simulation converges to the correct result by progressively increasing its density until no variations in the calculated solution are achieved. Adaptive mesh refinement is employed to handle the fine details of the microstrip feed line and the edges of the radiating patch, ensuring high accuracy in the calculation of the input impedance.

The starting point of the synthesis is the printed diamond-shaped patch monopole, which has been preliminarily designed to achieve a low reflection coefficient in a range centered around 1.5 GHz when operating in "free space" conditions. The optimization process involves a parametric sweep of the distance between the printed monopole and the corner vertex, as well as the opening angle of the reflector. It is observed that the distance L_1 plays a crucial role in impedance matching at the lower edge of the frequency band (1 GHz), while the side length T primarily influences the front-to-back ratio. Balancing these parameters is critical; moving the reflector too close to the monopole improves directionality but degrades the low-frequency matching due to capacitive coupling.

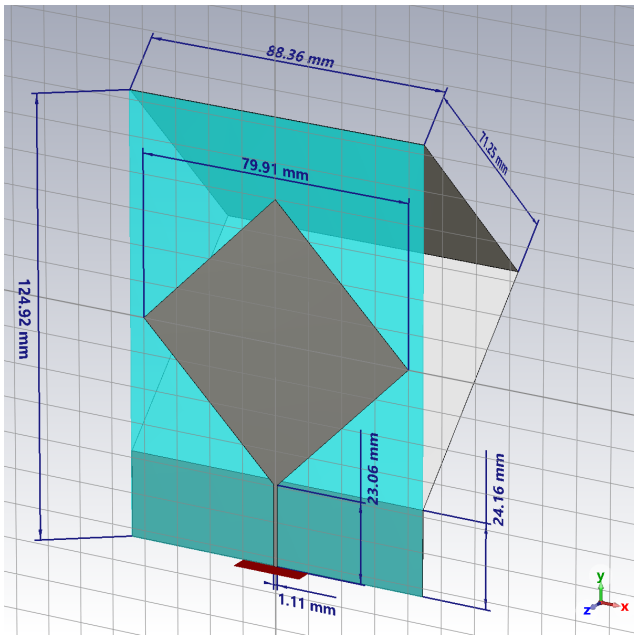

Figure 1. Screenshot of the CST model of the proposed antenna with dimensions.

In the final design, the radiating element is realized as a square diamond-shaped patch, with a diagonal $D = 79.91$ mm, on a rectangular substrate of DICLAD870, with relative permittivity $\epsilon_r = 2.33$, height $h = 0.508$ mm, of size $W = 88.36$ mm and $L_1 = 124.92$ mm. The choice of DICLAD870 is driven by its low loss tangent and stable dielectric properties, which are essential for maintaining efficiency and consistent performance across the designated bandwidth. A microstrip line of width $P = 1.11$ mm and length $L_2 = 23.06$ mm is connected to a waveguide port to simulate the use of a standard 50 Ω connector. The copper thickness on both sides of the DICLAD870 laminate is 35 µm. The right-angled triangular cavity has a side length of $T = 71.25$ mm, and is realized with a thin metal sheet. To improve the matching of the structure with the source, the substrate of the microstrip has a length of $L_3 = 24.16$ mm.

2.2. Numerical Verification

The simulated reflection coefficient of the antenna is shown in Figure 2. It shows a reflection lower $\Gamma \leq -10$ dB in the range 0.780–2.3 GHz, thus achieving a fractional bandwidth of approximately 100%. This threshold of −10 dB is standard for ensuring that at least 90% of the power delivered by the transmitter is accepted by the antenna, which is crucial for maximizing the dynamic range of the radar system. It is worth remarking that for narrowband antennas, it is usually possible to associate the main, usually very pronounced, local minima with the main electrical resonance of the structure; this reasoning may not be generally applied to wideband and ultra-wideband antennas as in the proposed design since multiple modes interact and generate complex reflection coefficient curves, so it may be challenging to associate the presence of local minima to specific geometrical features of the structure.

In Figure 3, we can see the RMS value of the electric field on the yx plane passing through the middle of the monopole for the frequency of 1.5 GHz, and we can see that the corner reflector significantly limits the field on the back side of the antenna. This shielding effect is a key design achievement, as it decouples the radiating element from the electronics and metallic structures of the drone located above the antenna. This behavior is confirmed by the plot of the radiation pattern of the antenna, at the frequency of 1.5 GHz, provided in Figure 4; this radiation pattern shows a wide main beam, suitable for the desired application of buried object detection, and shows a minimal radiation in the back direction, thus limiting the interference from the UAV carrying the antenna.

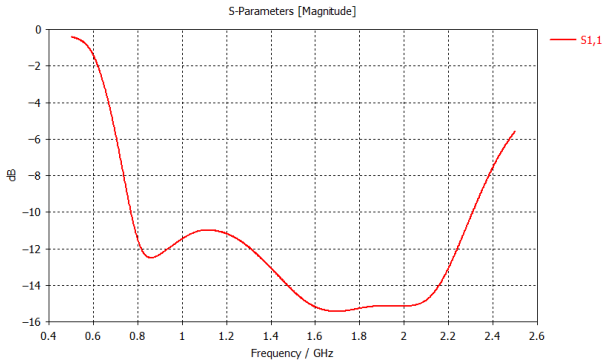

Figure 2. Simulated reflection coefficient of the antenna.

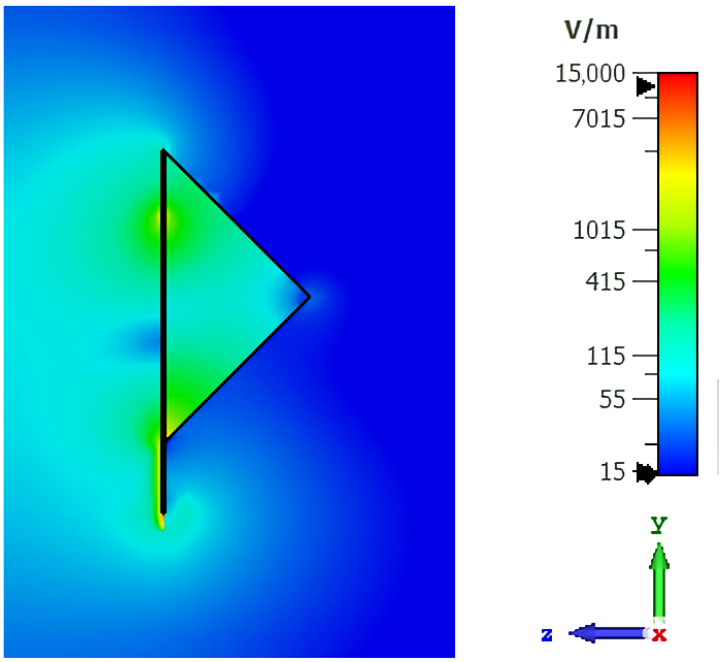

Figure 3. RMS value of the electric field of the antenna; yz cut plane, in the middle of the antenna.

The radiation pattern also shows excellent stability. In Figure 5 we can see the pattern of the antenna for some radiation frequencies between 1.0 GHz and 2.0 GHz; in this case, we have chosen to use the uv-plane (with $u = \sin\theta \sin\phi$ and $v = \sin\theta \cos\phi$) representation of the pattern to make the comparison among different patterns easier than the 3D polar representation used in Figure 4. The uv-plane representation projects the hemisphere onto a 2D plane, allowing for a more direct visual inspection of the beam width across the spectrum. It is worth underlining that the two representations are achieved in the same spherical coordinate system and are perfectly coherent. It is also interesting to note that the maximum gain exhibits a variation of less than 2 dB in the entire frequency range as evident in Table 1. We want to remark that the radiation pattern behavior in the frequency range 1.0 GHz and 2.0 GHz is very stable, and the pattern for intermediate frequencies not shown in Figure 5 could be achieved by means of interpolation.

Table 1. Variation of the maximum gain with frequency.

Frequency (GHz)	1.0	1.2	1.4	1.6	1.8	2.0
Realized Gain (dB)	4.4	5.1	5.8	6.0	6.3	6.1

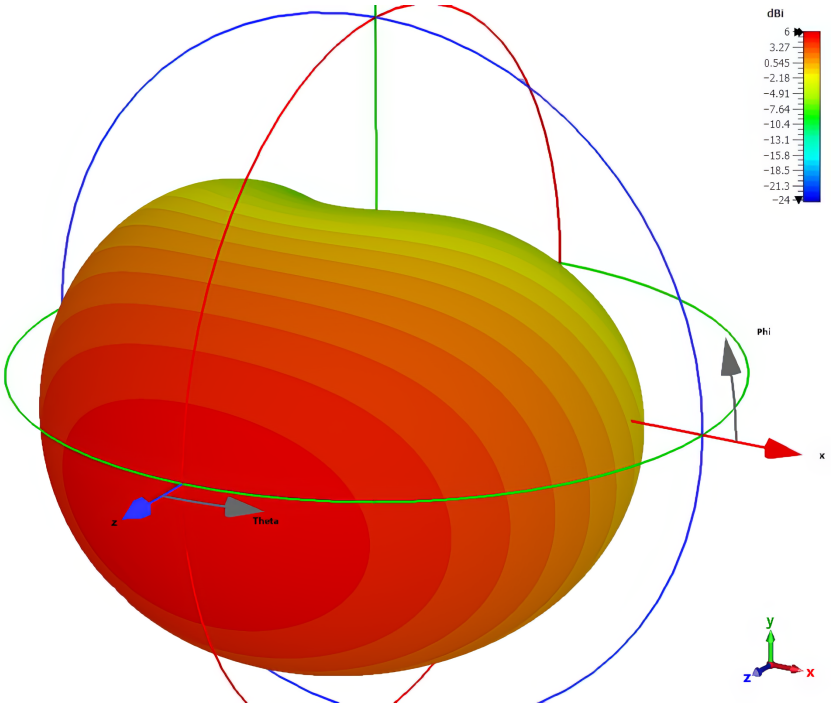

Figure 4. Radiation pattern of the antenna at the frequency of 1.5 GHz.

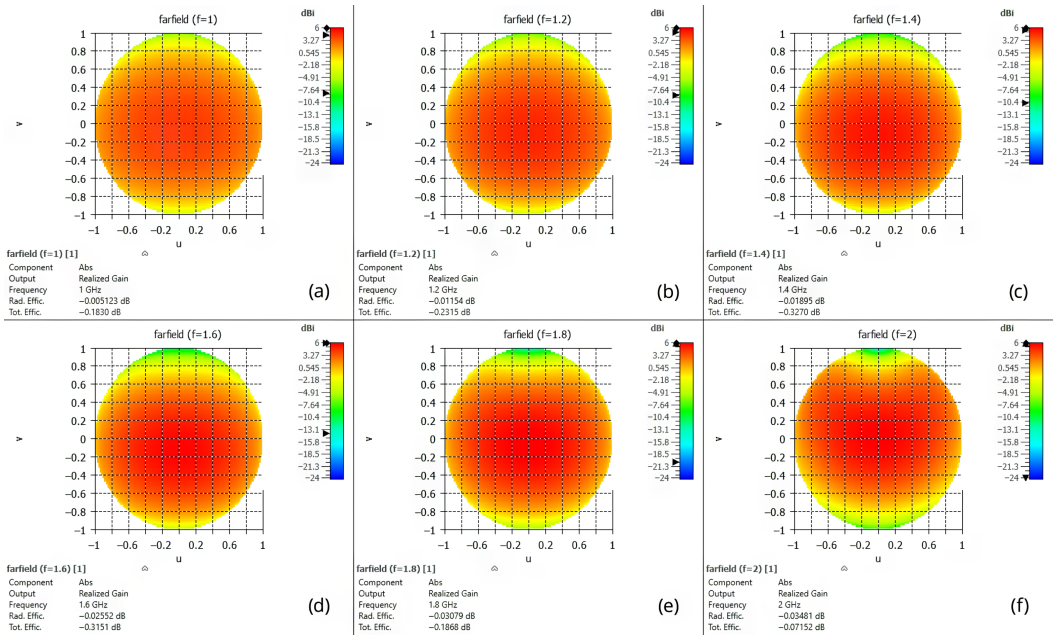

Figure 5. Variation of the pattern of the antenna in *uv*-plane for (**a**) 1.0 GHz, (**b**) 1.2 GHz, (**c**) 1.4 GHz, (**d**) 1.6 GHz, (**e**) 1.8 GHz and (**f**) 2.0 GHz.

To assess the feasibility of the antenna when used on a UAV, we conducted some numerical tests. These simulations show that the reflection coefficient of the antenna, as well as the radiation pattern, are not modified by the presence of the drone since, as shown in Figure 3, the back-radiated field is very limited. To clarify this point, in Figure 6 we can see the simulation at 1.5 GHz of the surface current in one of the considered worst cases: a drone, entirely made of metal, is loading the designed antenna on its bottom part, as it would during operation. A full-metal drone represents an extreme boundary condition, as most commercial UAVs utilize carbon fiber or plastic composites; therefore, if the antenna performs well in this scenario, it is guaranteed to perform well in real-world conditions. As we can see, the current

density is almost negligible, and it would have been even lower on a real UAV, which uses a large amount of plastic material to reduce the overall weight.

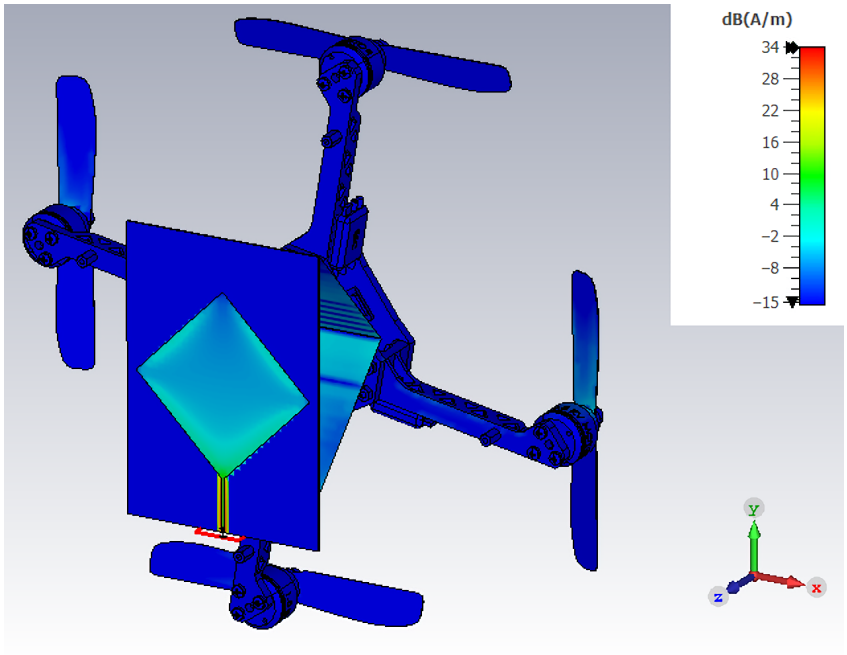

Figure 6. Plot of the surface current when a drone made of metal is loading the antenna.

Finally, we tested the antenna's capability to handle wideband signals correctly. In Figure 7, we can see the simulation of the group delay evaluated for a couple of the designed antennas, one facing the other, at a distance of 50 cm. It is possible to see that in the range 1–2 GHz, the delay spread is limited to about 200 ps, which is an adequate value for an antenna of this kind [14]. A flat or slowly varying group delay is synonymous with a linear phase response, which ensures that the different frequency components of the UWB pulse arrive simultaneously, maintaining the sharpness of the pulse in the time domain. The time-domain analysis of the radiated signals confirms minimal distortion and excellent signal fidelity.

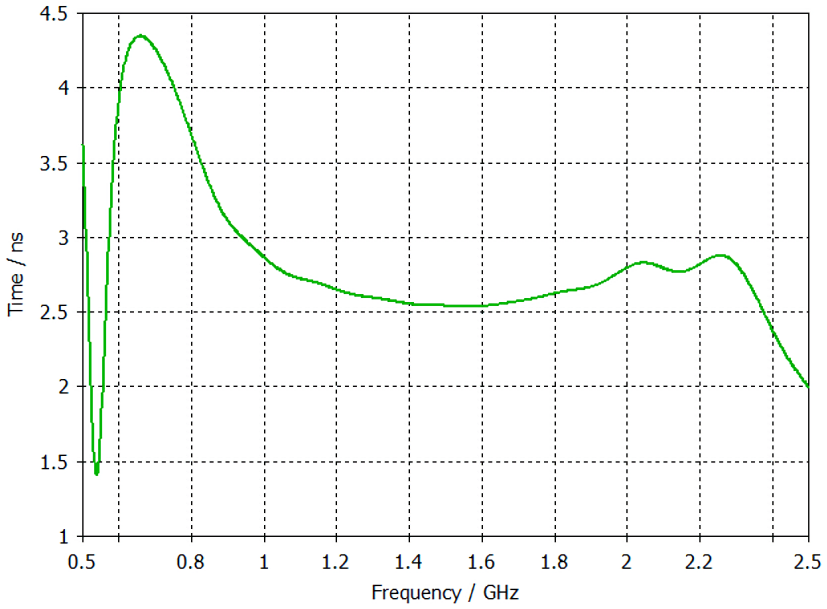

Figure 7. Simulated group delay for a couple of identical antennas, one facing the other, at a distance of 50 cm.

3. Prototype Construction and Measurements

Since the numerical simulation has shown promising behavior, we built a prototype of the antenna. The transition from simulation to physical realization involves practical manufacturing considerations that can influence the final performance, necessitating careful assembly and material selection.

The realization was achieved using a laminate of DICLAD870, of 0.508 mm thickness, with a copper metallization of 35 μm on both sides of the laminate. We first realized the diamond monopole antenna, with the same dimensions described in Figure 1. In order to use a standard SubMiniature version A (SMA) cable for driving the antenna, a SMA-to-line connector was soldered to the microstrip for the excitation of the antenna (see Figure 8). Particular care was taken during the soldering process to minimize impedance discontinuities at the transition between the coaxial connector and the planar microstrip line. The realized monopole can be seen in Figure 9.

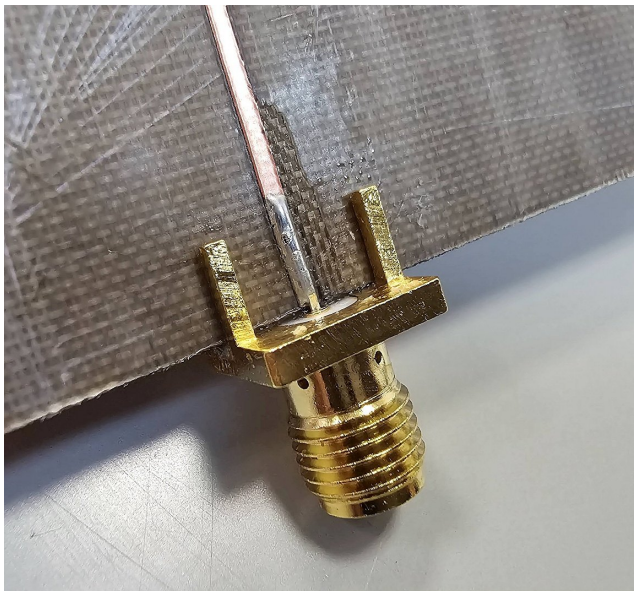

Figure 8. The SubMiniature version A (SMA) connector soldered to the stripline.

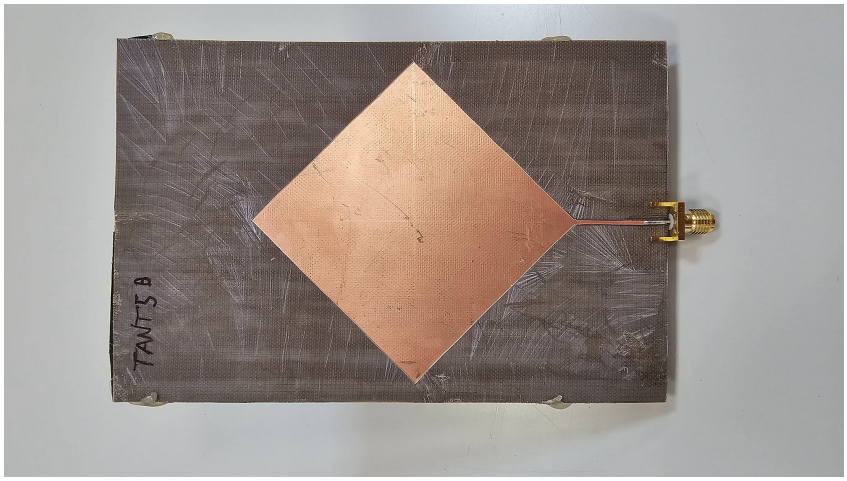

Figure 9. Photo of the realized prototype; front view of the diamond monopole.

In order to maximally reduce the weight of the antenna, the corner reflector was realized using the same substrate material employed for the realization of the monopole, and metal tape was used for connecting the reflector to the monopole as shown in Figure 10. The use of conductive copper tape enables rapid prototyping and adjustment of the elec-

trical connection between the planes. However, for a final industrial version, a single bent metallic sheet or a customized PCB bracket would be preferred to ensure long-term mechanical reliability and to provide greater resistance to vibrations typically encountered during UAV flights.

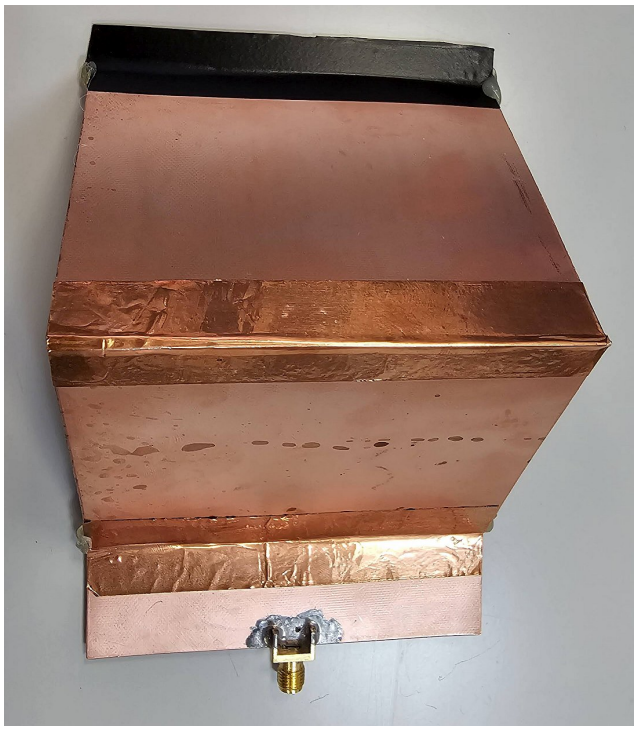

Figure 10. Photo of the realized prototype; back view of the corner reflector.

It must be noted that for achieving a mechanically stable antenna, the height of the monopole substrate was increased by 1 cm, in order to allow the use of an insulating taper for connecting the upper part of the corner reflector to the upper part of the monopole substrate. We have verified, through full-wave simulations, that this structural modification does not affect the electromagnetic behavior of the antenna. The overall antenna is shown in Figure 11; it is worth noting that the overall size of the antenna is limited, and the realized prototype weighs less than 40 g. This extremely low weight allows for the installation of additional sensors or larger batteries on the drone, thereby extending the mission duration.

Figure 11. Photo of the realized prototype; side view of the overall structure.

To facilitate the fabrication of the prototype, the size of the substrate supporting the diamond-shaped monopole was extended by 1 cm. This modification, necessary to simplify the assembly of the corner reflector, is visible in Figure 10, where the joint is secured by black tape. Numerical simulations confirmed that this structural adjustment does not affect the antenna's performance (reflection coefficient or radiation pattern), as the extension consists solely of dielectric material.

The built prototype was then tested using a vector network analyzer ZNA43.5 from Rohde Swartz, with a calibration kit ZV-Z229 and an SMA ruggedized test cable for connecting the antenna. The calibration process was performed up to the end of the cable to de-embed the cable losses and phase shifts, ensuring that the measured S-parameters accurately reflected the antenna's performance. The results of the measurement of the reflection coefficient, realized in free-space condition in the anechoic chamber of the University of Cassino, is provided in Figure 12. The response of the antenna matches very well with the simulations provided in Figure 2, and the artisanal construction can justify some minor differences. In particular, the handmade soldering of the connector to the microstrip line, as well as the use of metal tape, may have influenced the final result; an industrial rather than craft production process would likely remove these effects. However, the antenna prototype exhibits a reflection coefficient lower than −10 dB in the frequency range 1–2 GHz as requested.

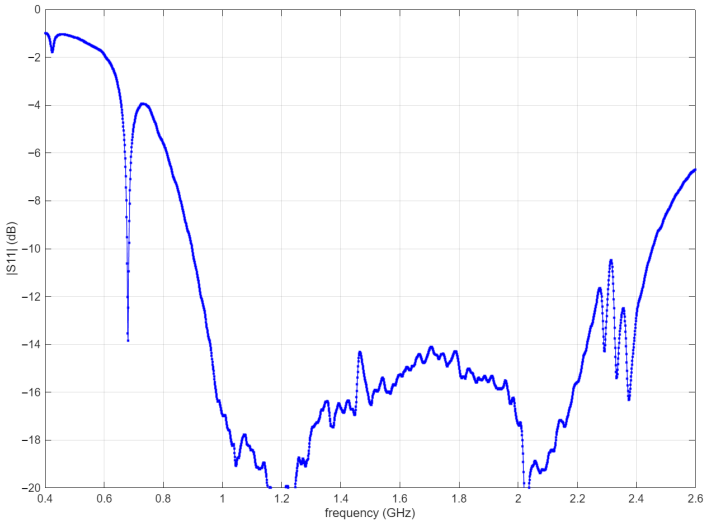

Figure 12. Measurement of the reflection coefficient of the antenna.

Table 2 presents a comparison of the proposed antenna with other systems found in the literature. It highlights that the proposed design achieves a superior balance between fractional bandwidth and weight compared to standard commercial GPR solutions and other experimental antennas. While other designs may offer wider bandwidths, they often do so at the cost of increased weight or complexity, or they lack the pattern stability required for reliable SAR imaging on moving platforms.

Table 2. Comparison with state-of-the-art UAV GPR antennas/systems.

Reference	Antenna/System Type	Bandwidth	Weight	Pattern Stability
[16]	3D Printed Horn	1–4 GHz	≈180 g	Medium
[27]	Cavity backed	2–6 GHz	not given	Medium–High
[25]	Planar reflector	0.5–1.3 GHz	not given	Medium
This Work	Corner Reflector	1–2 GHz	<40 g	High

4. Conclusions

In this contribution, we have introduced a novel radiating element, based on a monopole antenna connected to a corner reflector. The designed antenna exhibits a ultra-large fractional bandwidth, approaching 100%, and presents a very stable radiation pattern, which does not significantly change over the requested band of 1–2 GHz. This stability is a distinguishing feature that directly translates to improved image focusing in synthetic aperture radar applications. The numerical analysis shows a limited effect of the UAV loading the antenna, and a low distortion of the radiated signals.

The measurement of a realized prototype shows a reflection coefficient that agrees very well with the simulated one, confirming the validity of the overall design. The antenna, in particular, is very lightweight, weighing less than 40 g, and this value could be further reduced by its industrial realization. Such a reduction in payload mass is critical for small UAVs, allowing for extended flight times and wider area coverage in humanitarian demining missions.

As a further step, we are working towards the realization of antenna arrays using the same principle, possibly with a locally controllable environment [32]. Additionally, we are developing ground detection measurements in a software radio radar system that employs the proposed antenna. These advances are still in progress and will be discussed in a future paper.

Author Contributions: Conceptualization, D.P.; methodology, D.P. and M.D.M.; software, D.P.; hardware realization, D.P. and G.C.; validation, F.S., M.L. and G.C.; formal analysis, M.D.M.; investigation, F.S. and M.L.; resources, M.D.M.; data curation, G.C.; writing—original draft preparation, D.P.; writing—review and editing, F.S. and M.D.M.; visualization, G.C.; supervision, M.D.M.; project administration, M.D.M. and F.S.; funding acquisition, M.D.M. and F.S. All authors have read and agreed to the published version of the manuscript.

Funding: The research leading to these results has received funding from Project "Terrain" CUP H53D23007300001 funded by EU in NextGenerationEU plan through the Italian "Bando Prin 2022—D.D. 1409 del 14-09-2022" by MUR.

Institutional Review Board Statement: Not applicable.

Informed Consent Statement: Not applicable.

Data Availability Statement: The raw data supporting the conclusions of this article will be made available by the authors on request.

Acknowledgments: We would like to thank Jisan Miah for making the drone model used in the simulation available.

Conflicts of Interest: The authors declare no conflicts of interest. The funders had no role in the design of the study; in the collection, analyses, or interpretation of data; in the writing of the manuscript; or in the decision to publish the results.

References

1. Jol, H.M. *Ground Penetrating Radar Theory and Applications*; Elsevier: Amsterdam, The Netherlands, 2008.
2. Sato, M. Principles of mine detection by ground-penetrating RADAR. In *Anti-Personnel Landmine Detection for Humanitarian Demining: The Current Situation and Future Direction for Japanese Research and Development*; Springer: London, UK, 2009; pp. 19–26.
3. Garcia-Fernandez, M.; Alvarez-Lopez, Y.; Las Heras, F.; Gonzalez-Valdes, B.; Rodriguez-Vaqueiro, Y.; Pino, A.; Arboleya-Arboleya, A. GPR system onboard a UAV for non-invasive detection of buried objects. In Proceedings of the 2018 IEEE International Symposium on Antennas and Propagation & USNC/URSI National Radio Science Meeting, Boston, MA, USA, 8–13 July 2018; pp. 1967–1968.
4. Kasban, H.; Zahran, O.; Elaraby, S.M.; El-Kordy, M.; Abd El-Samie, F.E. A comparative study of landmine detection techniques. *Sens. Imaging Int. J.* **2010**, *11*, 89–112. [CrossRef]

5. Qiao, L.; Qin, Y.; Ren, X.; Wang, Q. Identification of buried objects in GPR using amplitude modulated signals extracted from multiresolution monogenic signal analysis. *Sensors* **2015**, *15*, 30340–30350. [CrossRef] [PubMed]
6. Daniels, D.J. *Ground Penetrating Radar*, 2nd ed.; IET: Stevenage, UK, 2009.
7. Garcia-Fernandez, M.; Alvarez-Lopez, Y.; Arboleya, A.; Gonzalez-Valdes, B.; Rodriguez-Vaqueiro, Y.; Las-Heras, F. Synthetic Aperture Radar Imaging System for Landmine Detection Using a Ground Penetrating Radar on Board a Unmanned Aerial Vehicle. *IEEE Access* **2018**, *6*, 45841–45851. [CrossRef]
8. Garcia-Fernandez, M.; López, Y.Á.; Andrés, F.L.-H. Airborne Multi-Channel Ground Penetrating Radar for Improvised Explosive Devices and Landmine Detection. *IEEE Access* **2020**, *8*, 165927–165943. [CrossRef]
9. Chen, Y.; Wang, C.F. Electrically small UAV antenna design using characteristic modes. *IEEE Trans. Antennas Propag.* **2013**, *62*, 535–545. [CrossRef]
10. Marques, P.; Martins, M.; Baptista, A.; Torres, J.P.N. Communication antenas for UAVs. *J. Eng. Sci. Technol. Rev.* **2018**, *11*, 90–102. [CrossRef]
11. Reis, S.; Silva, F.; Albuquerque, D.; Pinho, P. General Overview of Antennas for Unmanned Aerial Vehicles: A Review. *Electronics* **2025**, *14*, 3205. [CrossRef]
12. Cheraghinia, M.; Shahid, A.; Luchie, S.; Gordebeke, G.J.; Caytan, O.; Fontaine, J.; Herbruggen, B.V.; Lemey, S.; Poorter, E.D. A Comprehensive Overview on UWB Radar: Applications, Standards, Signal Processing Techniques, Datasets, Radio Chips, Trends and Future Research Directions. *IEEE Commun. Surv. Tutor.* **2025**, *27*, 2283–2324. [CrossRef]
13. Nowakowski, M.; Idzkowski, A. Ultra-wideband signal transmission according to European regulations and typical pulses. In Proceedings of the 2020 International Conference Mechatronic Systems and Materials (MSM), Białystok, Poland, 1–3 July 2020; pp. 1–4. [CrossRef]
14. Siwiak, K.; McKeown, D. *Ultra-Wideband Radio Technology*; John Wiley & Sons: Hoboken, NJ, USA, 2005.
15. Qu, S.W.; Li, J.L.; Xue, Q.; Chan, C.H. Wideband Cavity-Backed Bowtie Antenna with Pattern Improvement. *IEEE Trans. Antennas Propag.* **2009**, *56*, 3850–3854. [CrossRef]
16. Burr, R.; Schartel, M.; Mayer, W.; Walter, T.; Waldschmidt, C. Lightweight Broadband Antennas for UAV based GPR Sensors. In Proceedings of the 2018 15th European Radar Conference (EuRAD), Madrid, Spain, 26–28 September 2018; pp. 211–214. [CrossRef]
17. Wu, K.; Lambot, S. Analysis of low-frequency drone-borne GPR for root-zone soil electrical conductivity characterization. *IEEE Trans. Geosci. Remote Sens.* **2022**, *60*, 2006213. [CrossRef]
18. Schartel, M.; Burr, R.; Mayer, W.; Docci, N.; Waldschmidt, C. UAV-based ground penetrating synthetic aperture radar. In Proceedings of the 2018 IEEE MTT-S International Conference on Microwaves for Intelligent Mobility (ICMIM), Munich, Germany, 16–18 April 2018; pp. 1–4.
19. Linck, R.; Fassbinder, J.W.E. Testing the Applicability of Drone-Based Ground-Penetrating Radar for Archaeological Prospection. *Remote Sens.* **2024**, *16*, 1498. [CrossRef]
20. Ralston, J.; Hargrave, C. Software defined radar: An open source platform for prototype GPR development. In Proceedings of the 2012 14th International Conference on Ground Penetrating Radar (GPR), Shanghai, China, 4–8 June 2012; pp. 172–177.
21. Costanzo, S.; Di Massa, G.; Costanzo, A.; Borgia, A.; Raffo, A.; Viggiani, G.; Versace, P. Software-defined radar system for landslides monitoring. In *New Advances in Information Systems and Technologies*; Springer: Berlin/Heidelberg, Germany, 2016; Volume 2, pp. 325–331.
22. Guha, D.; Antar, Y.M. *Microstrip and Printed Antennas: New Trends, Techniques and Applications*; John Wiley & Sons: Hoboken, NJ, USA, 2011.
23. Ray, K.P. Design aspects of printed monopole antennas for ultra-wide band applications. *Int. J. Antennas Propag.* **2008**, *2008*, 713858. [CrossRef]
24. Cicchetti, R.; Miozzi, E.; Testa, O. Wideband and UWB antennas for wireless applications: A comprehensive review. *Int. J. Antennas Propag.* **2017**, *2017*, 2390808. [CrossRef]
25. Cao, P.; Huang, Y.; Zhang, J. A UWB monopole antenna for GPR application. In Proceedings of the 2012 6th European Conference on Antennas and Propagation (EUCAP), Prague, Czech Republic, 26–30 March 2012; pp. 2837–2840.
26. Chatterjee, A.; Parui, S.K. Performance enhancement of a dual-band monopole antenna by using a frequency-selective surface-based corner reflector. *IEEE Trans. Antennas Propag.* **2016**, *64*, 2165–2171. [CrossRef]
27. Edalati, A.; Shao, W.; McCollough, T.; McCollough, W. A novel cavity backed monopole antenna with UWB unidirectional radiation. *Prog. Electromagn. Res. C* **2017**, *72*, 1–13. [CrossRef]
28. Al-Gburi, A.J.A.; Ibrahim, I.M.; Zakaria, Z.; Abdulhameed, M.K.; Saeidi, T. Enhancing gain for UWB antennas using FSS: A systematic review. *Mathematics* **2021**, *9*, 3301. [CrossRef]
29. Pinchera, D.; Migliore, M.D.; Schettino, F. An ultra wide permittivity antenna (UWPA) for reliable through-wall communications. *IEEE Trans. Antennas Propag.* **2012**, *61*, 957–960. [CrossRef]

30. Yan, D.; Dang, Q.; Zhang, Z. Design of a cavity backed antenna operating at K band. In Proceedings of the 2025 6th International Conference on Electronic Communication and Artificial Intelligence (ICECAI), Chengdu, China, 20–22 June 2025; pp. 190–193.
31. Dassault Systèmes. *CST Studio Suite*, Version 2024; Dassault Systèmes: Waltham, MA, USA, 2024. Available online: https://www.3ds.com/products/simulia/cst-studio-suite (accessed on 13 January 2026).
32. Pinchera, D.; Lucido, M.; Chirico, G.; Schettino, F.; Migliore, M.D. Controllable Local Propagation Environment to Maximize the Multiplexing Capability of Massive MIMO Systems. *Electronics* **2023**, *12*, 2022. [CrossRef]